Frontiers in Bioscience Landmark

Front. Biosci. (Landmark Ed) **2026**; 31(2): 48779
https://doi.org/10.31083/FBL48779

Original Research

Integrative Analysis of Glycine, Serine, and Threonine Metabolism and the Immune Microenvironment in Endometrial Cancer: A Prognostic Model and Metabolic-Immune Framework for Precision Oncology

Jingxuan Ye[1,2,3,4], Yashi Shi[1,2,3,4], Xite Lin[1,2,3,4], Maotong Zhang[1,2,3,4], Xiaodan Mao[2,3,4,*], Pengming Sun[2,3,4,*]

[1]College of Clinical Medicine for Obstetrics & Gynecology and Pediatrics, Fujian Medical University, 350001 Fuzhou, Fujian, China
[2]Laboratory of Gynecologic Oncology, Fujian Maternity and Child Health Hospital, College of Clinical Medicine for Obstetrics & Gynecology and Pediatrics, Fujian Medical University, 350001 Fuzhou, Fujian, China
[3]Fujian Key Laboratory of Women and Children's Critical Diseases Research, Fujian Maternity and Child Health Hospital (Fujian Women and Children's Hospital), 350001 Fuzhou, Fujian, China
[4]Fujian Clinical Research Center for Gynecological Oncology, Fujian Maternity and Child Health Hospital (Fujian Obstetrics and Gynecology Hospital), 350001 Fuzhou, Fujian, China
*Correspondence: maodan1985@yeah.net (Xiaodan Mao); fmsun1975@fjmu.edu.cn; sunfemy@hotmail.com (Pengming Sun)
Academic Editor: Amancio Carnero Moya
Submitted: 3 December 2025 Revised: 8 January 2026 Accepted: 16 January 2026 Published: 11 February 2026

Abstract

Background: Metabolic reprogramming is a hallmark of the pathogenesis and progression of endometrial carcinoma (EC). This study comprehensively analyzed the expression profiles of glycine, serine, and threonine (Gly/Ser/Thr) metabolism–related genes in EC. We also established a robust prognostic model and developed a molecular subtyping framework that integrates metabolic and immune characteristics based on the identified prognostic genes. The aims of this work are to enhance diagnostic precision and improve clinical management strategies for patients with EC. **Methods**: Untargeted metabolomic analysis was performed on 35 EC and 15 normal tissues. The Cancer Genome Atlas (TCGA) transcriptomic data were integrated with weighted gene co-expression network analysis (WGCNA) to identify EC-related metabolic genes and construct a prognostic model using Cox proportional hazards and least absolute shrinkage and selection operator (LASSO) regression analyses. The model was validated using an independent proteomic and single-cell dataset from our institution. Consensus clustering classified patients into three molecular subtypes, which were further characterized by gene set variation analysis (GSVA) and profiling of immune infiltration. Finally, key prognostic genes were validated by reverse transcription quantitative polymerase chain reaction (RT-qPCR) in EC and normal endometrial epithelial cells. **Results**: Metabolomic analysis revealed significant enrichment of the Gly/Ser/Thr metabolic pathways. WGCNA identified a tumor-associated metabolic module among 1741 pathway-related genes. A prognostic model comprising methylenetetrahydrofolate dehydrogenase 2 (*MTHFD2*), ribosomal protein S6 kinase A1 (*RPS6KA1*), and cyclin-dependent kinase inhibitor 2A (*CDKN2A*) was subsequently established. Consensus clustering based on risk scores stratified EC patients into three molecular subtypes: immunometabolic-suppressed (C1), proliferative-immunobalanced (C2), and immune-activated (C3). The C1 subtype had the poorest prognosis and was characterized by metabolic suppression and immune evasion. The C2 subtype showed a favorable prognosis and was defined by a "proliferation–immune balance" in which high proliferative activity coexisted with strong anti-tumor immunity. The C3 subtype was also associated with a favorable outcome, driven by upregulated DNA repair and oxidative phosphorylation pathways alongside infiltration of immune-active cells. RT-qPCR confirmed significant differences in the mRNA expression of *MTHFD2*, *RPS6KA1*, and *CDKN2A* between normal and EC cells ($p < 0.05$). **Conclusion**: This study developed a Gly/Ser/Thr pathway–based prognostic model for EC, based on the expression of MTHFD2, RPS6KA1, and CDKN2A as novel biomarkers. The resulting patient stratification framework holds significant clinical potential for guiding precise and personalized management of EC.

Keywords: endometrial cancer; metabolic pathways; prognosis; biomarkers; bioinformatics

1. Introduction

Endometrial cancer (EC) represents a major global disease burden, with 420,242 newly diagnosed cases and 97,704 EC-related deaths worldwide in 2022. Both the incidence and mortality of EC continue to rise [1,2], and the growing prevalence of metabolic risk factors for EC is expected to further increase its incidence. While early-stage EC patients often achieve good outcomes through surgery, advanced cases still have high recurrence and mortality, with a five-year survival rate of <50% [3]. Furthermore, the current prognostic systems for EC fail to capture the full molecular complexity of this disease.

Metabolic reprogramming plays a key role in tumorigenesis and progression. Rapidly proliferating tumor cells require more energy and rely heavily on amino acids to support protein synthesis, nucleotide production, and redox

balance [4]. To meet these demands, tumor cells upregulate amino acid transporters (e.g., alanine, serine, cysteine transporter 2, L-type amino acid transporter 1) and metabolic enzymes (e.g., glutaminase, indoleamine 2,3-dioxygenase), effectively hijacking the hosts' amino acid resources [4–6]. This dependence on amino acid metabolism has emerged as a novel therapeutic target. Among the relevant pathways, the glycine-serine-threonine (Gly/Ser/Thr) axis has drawn attention due to its metabolic synergy in tumor progression. For instance, REV1 DNA directed polymerase promotes metabolic reprogramming by regulating the key enzyme cystathionine γ-lyase, leading to radiotherapy resistance in lung cancer [7]. Huang *et al.* [8] showed that serine protease inhibitor Kazal type I drives the progression of hepatocellular carcinoma through this pathway. Such findings highlight the Gly/Ser/Thr axis as a central driver of tumor proliferation, and suggest that targeting of this axis may disrupt tumor metabolic dependencies. However, the specific role of the Gly/Ser/Thr axis in EC remains largely unexplored.

Based on this, we conducted a systematic study of Gly/Ser/Thr pathway–related genes in EC to provide a theoretical foundation for building an EC-specific, metabolic-based prognostic model. This may lead to more precise patient stratification, which is an essential step toward precision medicine in EC.

2. Materials and Methods

2.1 Clinical Samples

This study included 99 endometrial samples, comprising 60 EC tissues and 39 matched normal endometrial tissues (non-malignant, collected within 2 cm of the tumor). Samples were obtained at Fujian Maternity and Child Health Hospital during routine clinical procedures. All patients provided written informed consent for their tissues to be used in this study.

Specifically, 35 EC samples and 15 normal endometrial samples were used for metabolomics analysis. A further 24 EC samples and 23 matched adjacent normal endometrial tissues were used for proteomics analysis. The final EC sample and paired adjacent normal endometrial tissue were used for single-cell RNA sequencing. The datasets were generated from independent sample cohorts, with no overlap among different omics analyses.

2.2 Untargeted Metabolomics

After collection, EC and adjacent normal tissues (**Supplementary Table 1**) were numbered, weighed, and placed in EP tubes. Extraction buffer (methanol: acetonitrile: water = 2:2:1, with isotope-labeled standards) was added to the samples, which were then homogenized and sonicated in cycles. They were subsequently incubated at –40 °C for 1 h and then centrifuged at 12,000 rpm for 15 minutes at 4 °C. The supernatant was transferred to glass vials for liquid chromatography-mass spectrometry/mass spectrometry analysis (Thermo Fisher Vanquish system, Waltham, MA, USA). Metabolomics analysis was performed by BIOTREE BIOTECH (Shanghai, China), and the metabolites were identified using an in-house database.

Differential metabolites were identified using two criteria: $p < 0.05$ and a variable importance in projection score >1 for the first principal component in the OPLS-DA model. Enrichment analysis of these metabolites was then conducted with reference to Kyoto Encyclopedia of Genes and Genomes (KEGG) and PubChem databases [9–11].

2.3 Dataset Acquisition

The study workflow is shown in **Supplementary Fig. 1**. TCGA-Uterine Corpus Endometrial Carcinoma (UCEC) data were obtained from The Cancer Genome Atlas, GSE17025 data from the Gene Expression Omnibus (GEO), and PDC000125 data from the CPTAC database.

2.4 Weighted Gene Co-Expression Network Analysis (WGCNA)

Using the WGCNA package (Version 1.73, Bioconductor, USA) [12], 539 tumor samples and 35 normal samples from TCGA-UCEC were analyzed to find gene modules linked to EC development. We started by selecting the top 25% most variable genes and calculating a Pearson correlation matrix based on mRNA data. After clustering samples to identify outliers, the optimal soft threshold (β) was determined for network construction. The correlation matrix was converted into a topological overlap matrix, and dynamic tree cutting was used for hierarchical clustering to group co-expressed genes into modules.

2.5 Differential Expression Analysis

The limma package (Version 3.58.1, Bioconductor, USA) [13] was used for differential expression analysis of TCGA-UCEC and GEO data, with screening criteria of $|\log2\text{-fold change}| \geq 1$ and adjusted $p < 0.05$.

2.6 Consensus Clustering

The ConsensusClusterPlus package (Version 1.66.0, Bioconductor, USA) [14] was used for consensus clustering analysis, with 1000 iterations for stability and reproducibility. The principal component analysis (PCA) method determined the optimal cluster number (k = 2–10), and the internal consistency index assessed the clustering stability. PCA was used to evaluate subtype separation based on expression patterns. Survival analysis was performed using the survival (Version 3.5.7, CRAN, Vienna, Austria) and survminer (Version 0.4.9, CRAN, Vienna, Austria) packages to compare prognostic outcomes across EC subtypes.

2.7 Construction of the Prognostic Model

A total of 537 patients with survival data were selected from the TCGA database and randomly split into training and test sets at a 7:3 ratio. Univariate Cox regression was

used to analyze 90 key metabolic genes for survival associations, identifying significant prognostic genes. Least absolute shrinkage and selection operator (LASSO) regression further filtered prognosis-related genes, and common genes from both methods were analyzed with multivariate Cox regression. The prognostic model was built using LASSO-Cox regression. The risk score was calculated using the following formula: $\sum$ (Xi * Yi) (X: coefficient, Y: gene expression level). Kaplan-Meier (K-M) curves were used to compare survival across risk groups, and risk-survival curves for mortality rates. To validate the model, receiver operating characteristic (ROC) analysis at 1, 3, and 5 years was performed using the survival (Version 3.5.7, CRAN, Vienna, Austria), survminer (Version 0.4.9, CRAN, Vienna, Austria), and timeROC packages (Version 0.4, CRAN, Vienna, Austria) [15].

2.8 Tumor Mutation Burden (TMB)

The maftools package (Version 2.18.0, Bioconductor, USA) was used to retrieve tumor mutation data for UCEC patients from the TCGA database. The mutation status of different risk populations was analyzed, and the combined effects of risk scores and TMB on patient survival outcomes were examined.

2.9 Analysis of Immune Cell Infiltration in the Tumor Microenvironment

Tumor immune dysfunction and exclusion (TIDE) scores for UCEC patients were obtained from the TIDE database. The chi-square test was used to assess differences in immunotherapy responses between different risk groups of EC patients. The CIBERSORT algorithm [16] was employed to assess differences in the levels of infiltrating immune cells in the tumor microenvironment (TME). The limma package was used for differential expression analysis of several classical immune checkpoint genes, while the estimate package (Version 1.0.13, CRAN, Vienna, Austria) was used to evaluate the TME.

2.10 Proteomics Analysis

Formalin-fixed, paraffin-embedded tissue samples were deparaffinized with xylene and ethanol, then homogenized in lysis buffer containing Tris-hydrochloride, dithiothreitol, and sodium dodecyl sulfate. After incubation at 99 °C for 60 minutes, the samples underwent ultrasonication, centrifugation, iodoacetamide alkylation, and acetone precipitation. Proteins were resuspended in 8M urea and analyzed by mass spectrometry using DIA-NN (Version 1.8, Berlin, Germany) with a false discovery rate set at 1%. Fisher's exact test and Pearson's test identified differentially expressed proteins ($p < 0.05$), with fold-changes $\geq$1.2 or $\leq$1/1.2 considered significant.

2.11 Single-Cell Transcriptomics Analysis

Fresh tumor tissues were cut into 1–3 mm^3 fragments and single-cell suspensions subsequently prepared using a single-cell 3′ Library and Gel Bead Kit V3.1 (10x Genomics, Pleasanton, CA, USA). Following enzymatic digestion and cell purification, the cell viability exceeded 90%, with a final cell concentration of 700–1200 cells/μL. Gel bead-in-emulsions (GEMs) were generated using a Chromium Single-Cell G Chip Kit (10x Genomics, Pleasanton, CA, USA), after which cell lysis, reverse transcription with unique molecular identifiers (UMIs), cDNA amplification, fragmentation, end repair, and adapter ligation were sequentially performed according to the manufacturer's protocol. The resulting libraries were sequenced on the Illumina platform. Raw sequencing data were processed using Cell Ranger (10x Genomics, Pleasanton, CA, USA) for read alignment, barcode processing, and UMI counting. Downstream analyses were performed in Seurat (Version 4.3.0, CRAN, Vienna, Austria), including quality control (cells with >200 detected genes and $\leq$25% mitochondrial gene expression), normalization, PCA, and uniform manifold approximation and projection (UMAP). This enabled cell type identification and characterization of subpopulations.

2.12 Gene Set Variation Analysis (GSVA)

GSVA was conducted to evaluate enrichment with hallmark pathways using the GSVA package (Version 1.50.0, Bioconductor, USA). Hallmark gene sets were obtained from MSigDB through the msigdbr package (Version 7.5.1, CRAN, Vienna, Austria) and converted to Entrez IDs to match the RNA-seq expression matrix. Differential pathway activity between groups was analyzed with limma using empirical Bayes moderation, with significance defined as $p < 0.05$ and $|T| > 2$.

2.13 Cell Line Construction and Culture

All cell lines were maintained in culture media containing 10% fetal bovine serum (FBS; Gibco, MT, USA) and 1% antibiotic–antifungal mixture (Basal Media, Shanghai, China). HEC-1A cells (KeyGEN BioTECH, Nanjing, China) were grown in McCoy's 5A medium without sugar and supplemented with glucose (Procell Life Science & Technology Co., Ltd., Wuhan, China). Ishikawa cells (KeyGEN BioTECH, Nanjing, China) were maintained in RPMI-1640 medium containing glucose (Procell Life Science & Technology Co., Ltd., Wuhan, China), whereas endometrial epithelial cells (EECs) (Whelab, Shanghai, China) were cultured in MEM supplemented with non-essential amino acids (NEAA; Procell Life Science & Technology Co., Ltd., Wuhan, China). All cell lines were maintained at 37 ℃ in a humidified atmosphere, validated by STR profiling, and tested negative for mycoplasma (Biowing Biotechnology Co., Ltd., Shanghai, China).

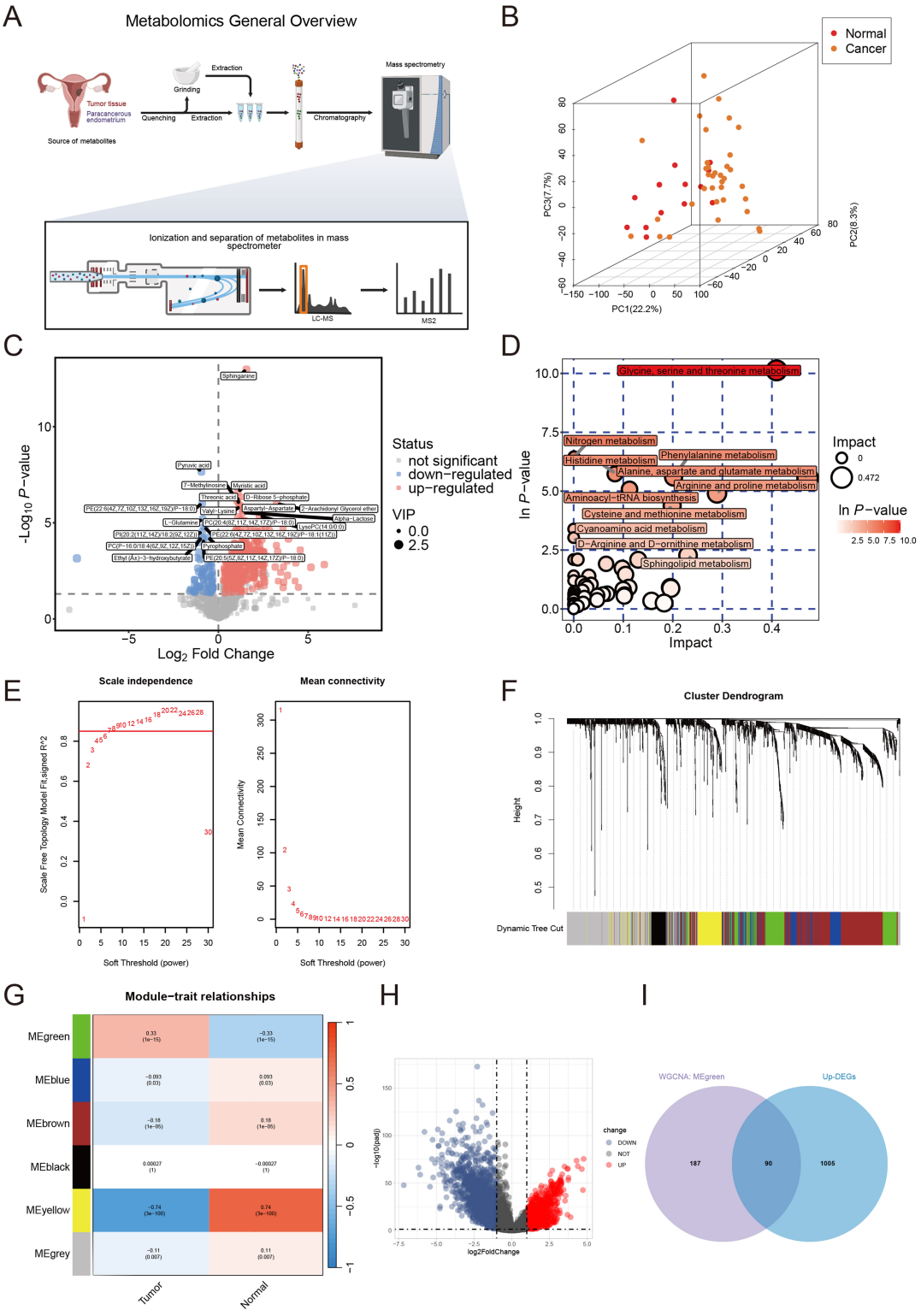

Fig. 1. Metabolomics and WGCNA analysis for the screening of Gly/Ser/Thr metabolism-related genes. (A) Metabolomics workflow. This figure was created in BioRender (https://BioRender.com/tkklo3h). (B) 3D PCA score scatter plot. (C) Volcano plot of differential metabolites. (D) Enrichment pathway map of differential metabolites. (E) Scale independence and mean connectivity analysis for soft-thresholding selection. (F) Gene dendrogram and module color assignment. (G) Module-trait relationship heatmap. (H) Volcano plot of DEGs. (I) Venn diagram of overlapping genes. LC-MS, liquid chromatography-mass spectrometry; MS2, secondary mass spectrometry; PCA, principal component analysis; WGCNA, weighted gene co-expression network analysis; Gly/Ser/Thr, glycine, serine, and threonine; DEGs, differentially expressed genes.

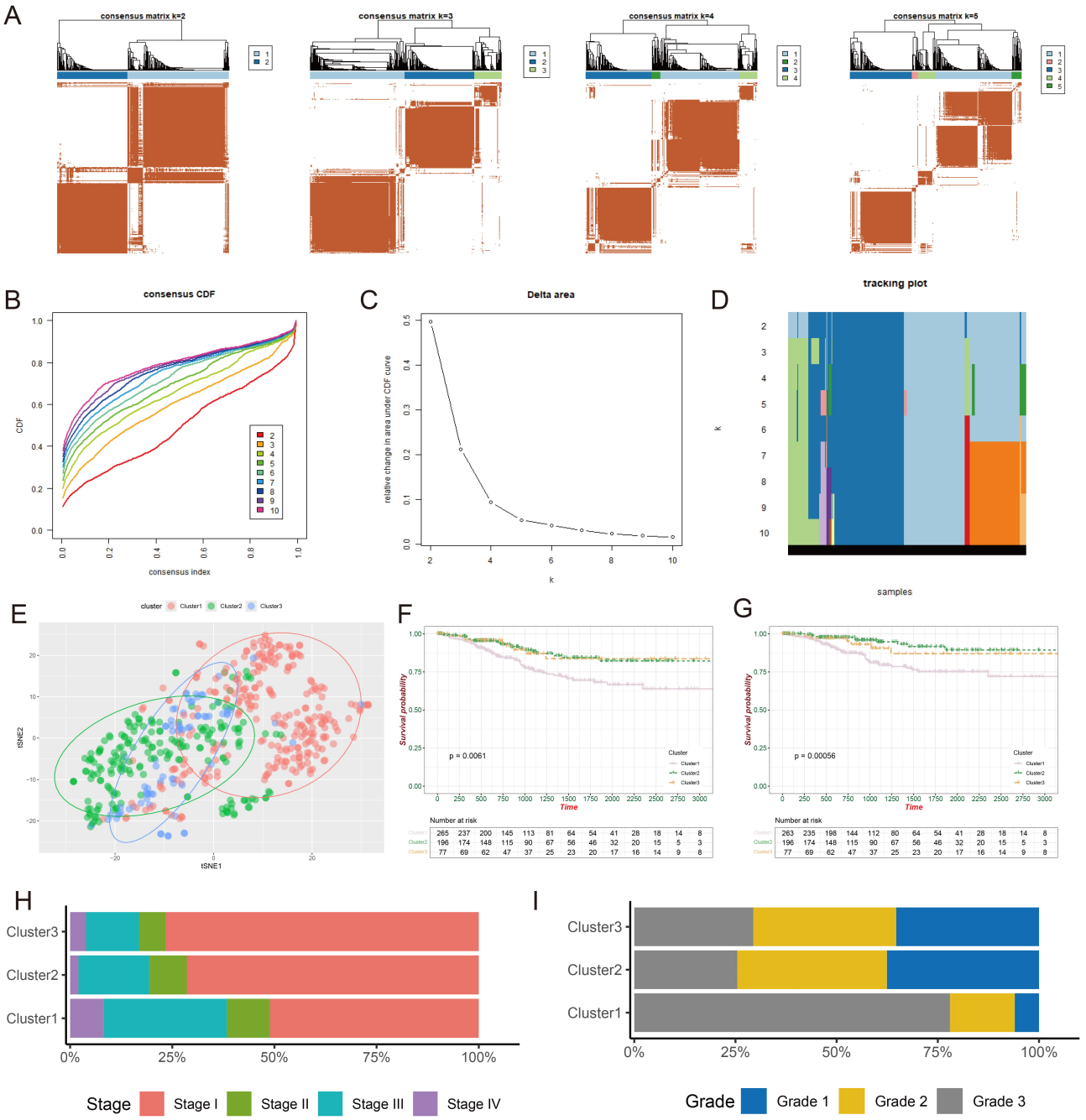

Fig. 2. Identification of Gly/Ser/Thr metabolism-related subtypes. (A) Consensus clustering matrices for k = 2–5. (B) CDF curves for k = 2–10. (C) Relative change in the area under the CDF delta curve. (D) Tracking plot for k = 2–10. (E) PCA demonstrating three distinct subgroups. (F,G) Differences in OS and DSS among the three subtypes. (H,I) Bar plots illustrating the distribution of different pathological grades and FIGO stages across subtypes. CDF, cumulative distribution function; PCA, principal component analysis; OS, overall survival; DSS, disease-specific survival; FIGO, International Federation of Gynecology and Obstetrics.

2.14 RT-qPCR

Cells were lysed directly in the culture dishes using RNA extraction reagent, and the lysates were thoroughly vortexed. After centrifugation, the supernatant was collected into a new tube. For phase separation, 0.25 mL of chloroform was added to every 1 mL of the extraction reagent. Following another centrifugation, the upper aqueous phase was carefully transferred to a clean tube. RNA was precipitated with isopropanol and subsequently washed with 75% ethanol. First-strand cDNA synthesis was carried out according to the manufacturer's instructions. Following preparation of the PCR master mix (Promega, Madison, WI, USA), quantitative PCR was conducted using the Eastep qPCR Master Mix (Promega, USA). The primer sequences

are shown in Table 1. GAPDH was used as the reference gene to determine relative gene expression levels with the $2^{-\Delta\Delta CT}$ method.

Table 1. Primer sequences used for RT-qPCR.

Primer		Sequence 5′-3′
CDKN2A	F	TCGCGATGTCGCACGGTA
	R	CAATCGGGGATGTCTGAGGGAC
MTHFD2	F	GATCCTGGTTGGCGAGAATCC
	R	TCTGGAAGAGGCAACTGAACA
RPS6KA1	F	CACCATTGGCAAAACTGTGG
	R	TGTAGCAAGGTGTCATGAGGAG
GAPDH	F	CGAAGGTGGAGTCAACGGATTT
	R	ATGGGTGGAATCATATTGGAAC

CDKN2A, cyclin-dependent kinase inhibitor 2A; *MTHFD2*, methylenetetrahydrofolate dehydrogenase 2; *RPS6KA1*, ribosomal protein S6 kinase A1.

2.15 Statistical Analysis

Statistical analyses were conducted in R (Version 4.3.1, R Foundation for Statistical Computing, Vienna, Austria) and GraphPad Prism 9.5 (GraphPad Software, San Diego, CA, USA), with data visualized using ggplot2 (Version 3.5.2, CRAN, Vienna, Austria) and ggpubr (Version 0.6.0, CRAN, Vienna, Austria). Group comparisons were carried out with Student's *t*-test (normal data), Wilcoxon rank-sum test (non-normal data), and Kruskal-Wallis test (multiple groups). Chi-square tests were used for categorical variables. Survival analyses were performed with the K-M method. Results with $p < 0.05$ were considered statistically significant.

3. Results

3.1 Differential Expression of Gly/Ser/Thr Metabolism-Related Genes in Tumor and Normal Tissues

We performed metabolomic analysis to investigate whether metabolic reprogramming occurs in EC (Fig. 1A). PCA revealed distinct metabolic profiles between EC and normal endometrial tissues (Fig. 1B). Subsequent differential analysis identified 4529 upregulated and 3222 downregulated metabolites (Fig. 1C). Pathway enrichment analysis revealed significant enrichment of the Gly/Ser/Thr metabolism pathways (Fig. 1D). We then screened for genes associated with this pathway, and identified and matched 1741 genes with relevance scores >10 through the GeneCards database (**Supplementary Table 2**). WGCNA was performed on the TCGA dataset, with a soft threshold of $\beta = 7$ ($R^2 = 0.85$) to construct a scale-free network (Fig. 1E,F). Six distinct modules were identified (Fig. 1G), among which the green module exhibited the strongest correlation with tumor tissues and contained 277 genes. Differential analysis of tumor and normal tissues identified 1095 up-regulated genes ($\log_2|\text{fold change}| > 1$, adjusted $p < 0.05$) (Fig. 1H). Intersection analysis of Gly/Ser/Thr metabolism–related WGCNA module genes and up-regulated differentially expressed genes (DEGs) in EC yielded 90 candidate genes (Fig. 1I).

3.2 EC Subtype Classification Based on Gly/Ser/Thr Metabolic Pathways

Unsupervised clustering analysis was performed on 539 EC tissues from the TCGA database using expression profiles of Gly/Ser/Thr metabolism-related genes. Optimal clustering stability was achieved at k = 3 (Fig. 2A–D), dividing patients into three distinct subgroups (C1: n = 266; C2: n = 196; C3: n = 77). PCA revealed significant transcriptomic heterogeneity among clusters (Fig. 2E). Survival analysis demonstrated pronounced prognostic heterogeneity, with C1 exhibiting the shortest overall survival (OS) and disease-specific survival (DSS) (Fig. 2F,G). Notably, C1 contained significantly higher proportions of advanced International Federation of Gynecology and Obstetrics (FIGO) stage (III/IV) and high-grade (G3) tumors (Fig. 2H,I), indicating greater clinical aggressiveness.

3.3 Immune Evasion and Immune Cell Infiltration in Different Subtypes

Consistent with established literature demonstrating metabolic-driven immune evasion in the TME [17,18], analysis of immune cell infiltration revealed distinct imbalances in the C1 phenotype, with increased Th2 cells and decreased activated $CD8^+$ T cells, DCs, NK cells, and myeloid-derived suppressor cells (MDSCs) (Fig. 3A). This phenotype likely reflects STAT6 pathway activation via Th2-secreted IL-4/IL-13, promoting M2 macrophage polarization and immunosuppression [19]. Concurrent DC dysfunction may impair antigen presentation and $CD8^+$ T cell activation [20], while NK cell exhaustion compromises innate immune surveillance, collectively facilitating metastatic dissemination. In contrast, C2 showed enhanced anti-tumor immunity with activated $CD4^+$ T cells and DCs, while C3 had an immunomodulatory environment dominated by NK cells, mast cells, and Tregs. Immunocheckpoint analysis showed significant upregulation of CD274 (*PD-L1*), lymphocyte activation gene 3 (*LAG3*), T-cell immunoreceptor with Ig and ITIM domains (*TIGIT*), and interferon gamma receptor 1 (*IFNGR1*) in C1 (Fig. 3B). Moreover, C1 demonstrated the lowest immune score, the highest TIDE score (Fig. 3C,D), elevated tumor purity, and a lower stromal score (Fig. 3E,F), suggesting an immunosuppressive environment with poor response to immunotherapy.

3.4 Development of a Metabolism-Related Prognostic Risk Model

To evaluate the prognostic significance of metabolic genes, we developed a prognostic model using data from

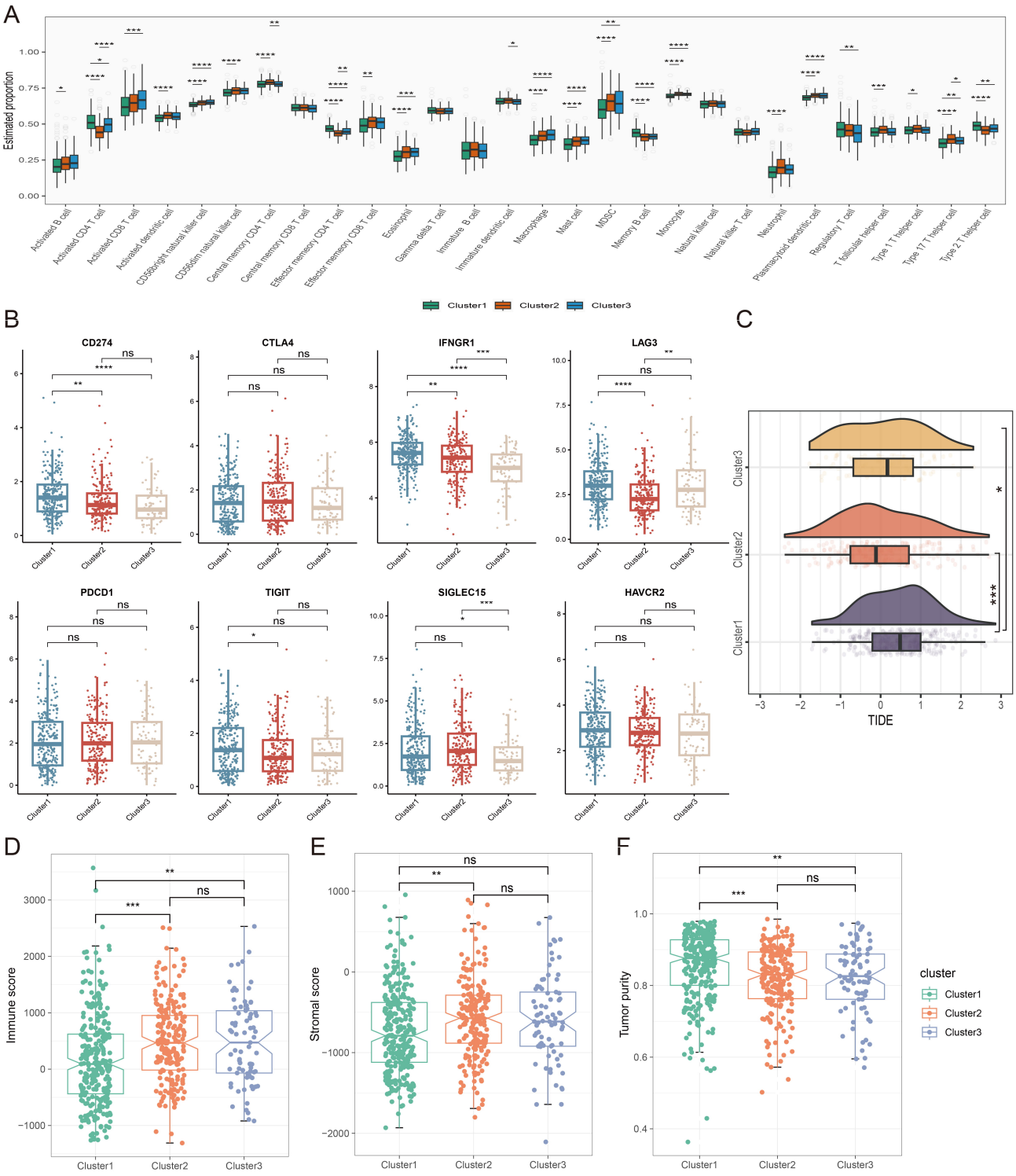

Fig. 3. Immune analysis of the different metabolic subtypes. (A) Comparison of infiltration levels of immune cell types among the three metabolic subtypes. (B) Expression levels of immune checkpoint-related genes in the three metabolic subtypes. (C–F) Evaluation of TIDE score (C), immune score (D), stromal score (E), and tumor purity score (F) in the three metabolic subtypes. ns, not significant, * $p < 0.05$, ** $p < 0.01$, *** $p < 0.001$, **** $p < 0.0001$. TIDE, tumor immune dysfunction, and exclusion; *LAG3*, lymphocyte activation gene 3; *TIGIT*, T-cell immunoreceptor with Ig and ITIM domains; *IFNGR1*, interferon gamma receptor 1; *CTLA-4*, cytotoxic T-lymphocyte-associated protein 4; *PDCD1*, programmed cell death 1; *SIGLEC15*, sialic acid-binding Ig-like lectin 15; *HAVCR2*, hepatitis A virus cellular receptor 2.

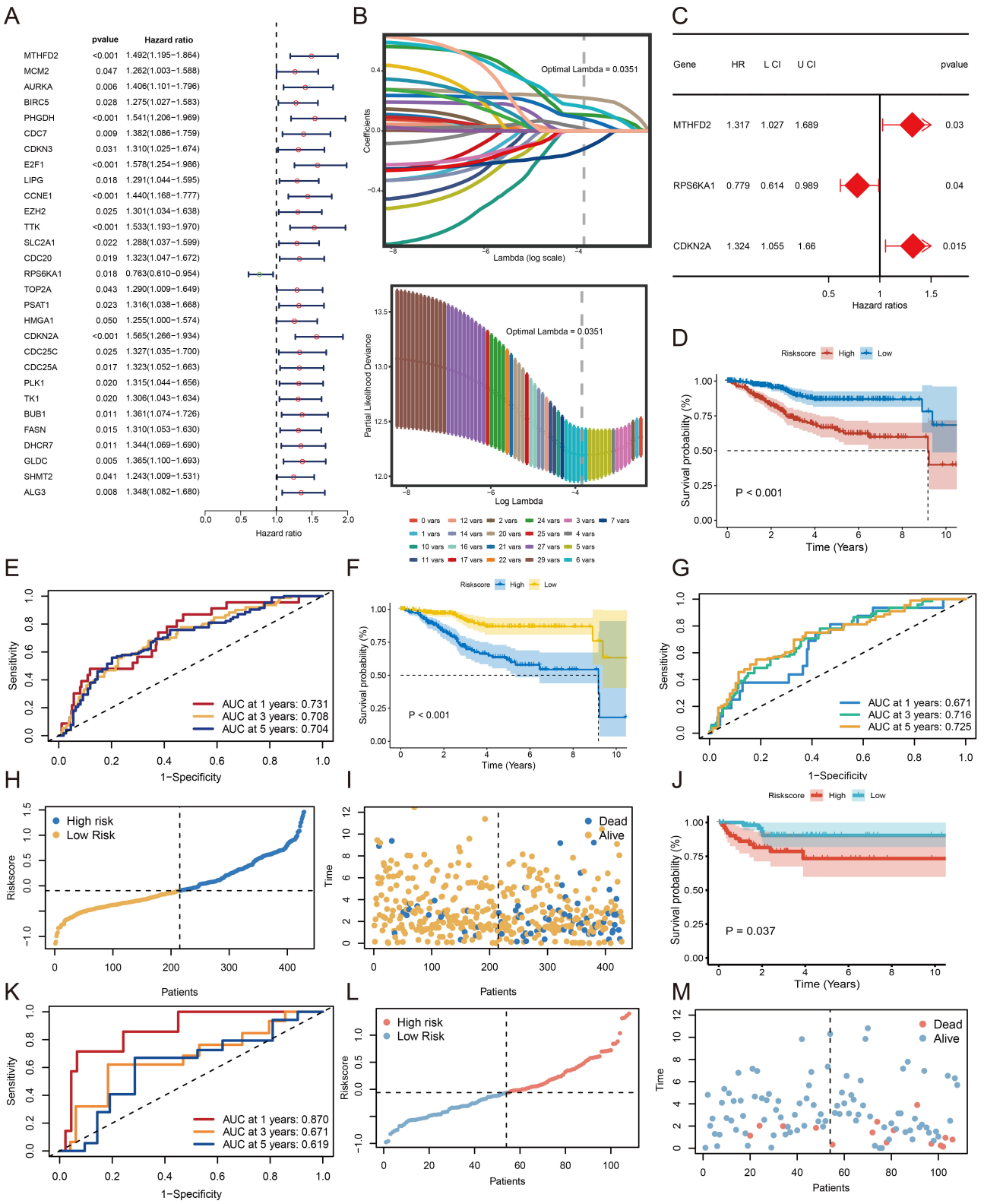

Fig. 4. Construction and validation of the risk prediction model. (A) Identification of genes associated with OS. (B) Variable selection in the LASSO model. (C) Determination of the most relevant genes. (D,F,J) K-M survival analysis comparing high- and low-risk groups. (E,G,K) Time-dependent ROC curves for predicting 1-, 3-, and 5-year survival rates. (H,I,L,M) Distribution of risk scores and survival status for each patient. OS, overall survival; LASSO, least absolute shrinkage and selection operator; K–M, Kaplan–Meier; ROC, receiver operating characteristic.

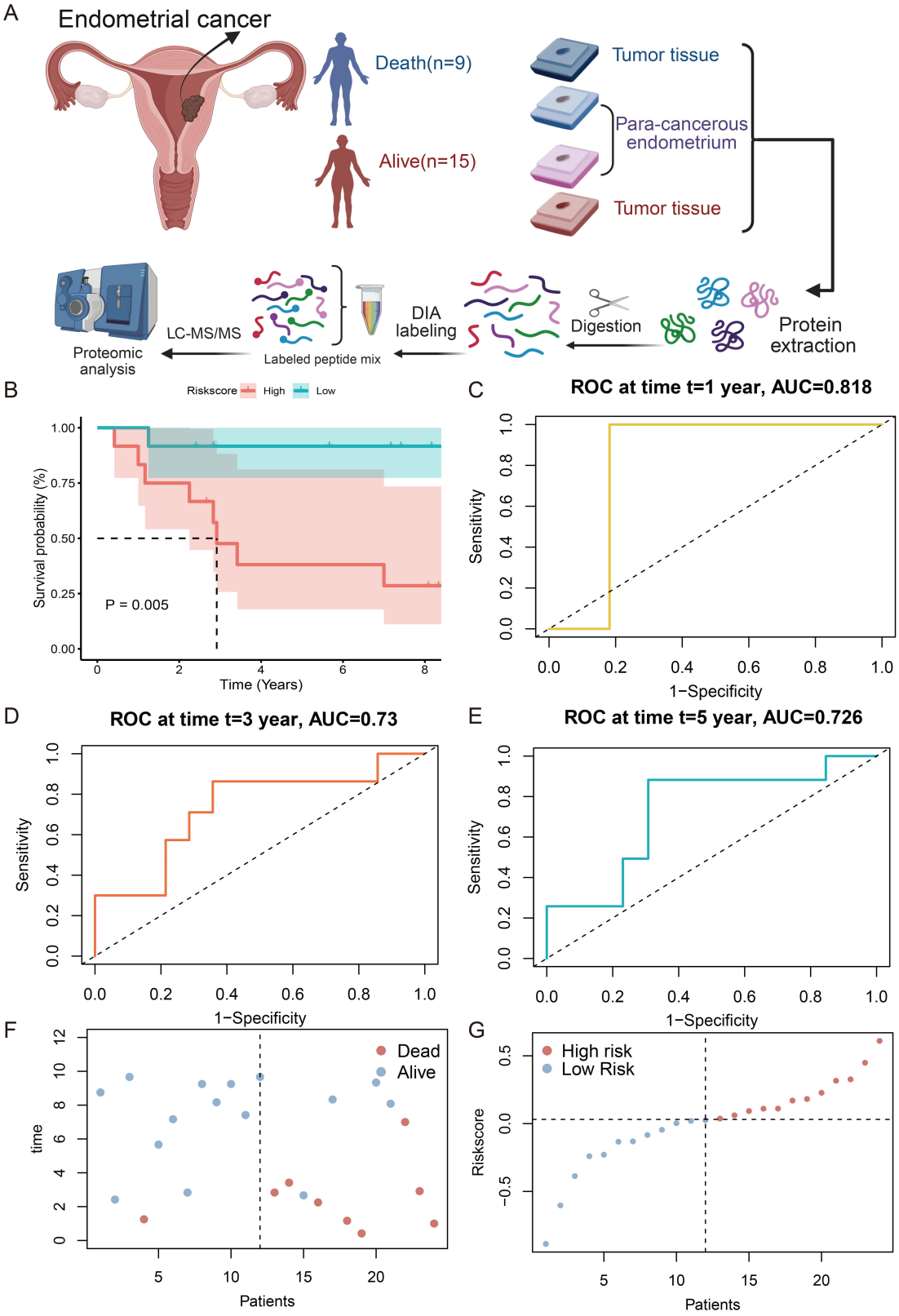

Fig. 5. Validation of the risk model through proteomics. (A) Workflow for the proteomics study. This figure was created in BioRender (https://BioRender.com/tkklo3h). (B) K-M survival analysis comparing high- and low-risk groups. (C–E) Time-dependent ROC curves for predicting 1-, 3- and 5-year survival rates. (F,G) Distribution of risk scores and survival status for each patient. K–M, Kaplan–Meier; ROC, receiver operating characteristic.

537 TCGA-UCEC cases. These were randomly divided into training (n = 429) and test (n = 108) cohorts at a ratio of 7:3. Univariate Cox regression identified 29 OS-associated metabolic genes (Fig. 4A, **Supplementary Table 3**). These were narrowed to 6 via LASSO-Cox regression (λ = 0.0351; Fig. 4B, **Supplementary Table 4**), and then further refined to three core genes (methylenetetrahydrofolate dehydrogenase 2 (*MTHFD2*), ribosomal protein S6 kinase A1 (*RPS6KA1*), cyclin-dependent kinase inhibitor 2A (*CDKN2A*)) using multivariate Cox analysis (Fig. 4C). The risk score was calculated as: (0.275 × *MTHFD2* expression) + (–0.249 × *RPS6KA1* expression) + (0.28 × *CDKN2A* expression). Patients were stratified into high- and low-risk groups based on their median risk score (**Supplementary Table 5**). K-M analysis revealed significantly worse OS in the high-risk group ($p < 0.001$, Fig. 4D). ROC analysis confirmed high predictive accuracy, with the area under the curve (AUC) >0.7 for 1-, 3-, and 5-year OS (Fig. 4E). In both the test cohort and the overall dataset, high-risk scores correlated with poorer survival ($p < 0.05$), with AUC >0.6 (Fig. 4F,G,J,K). Scatter plots further showed increased EC patient mortality with higher risk scores (Fig. 4H,I,L,M). Together, these results indicate the three-gene model (*MTHFD2*, *RPS6KA1*, *CDKN2A*) is a reliable predictor of EC prognosis.

3.5 Validation of the Prognostic Model by Proteomics

Tumor samples from 24 EC patients with different prognoses were analyzed by proteomic profiling (Fig. 5A). Stratifying patients by risk scores revealed the high-risk group had significantly worse survival ($p < 0.05$, Fig. 5B). AUC values for predicting 1-, 3-, and 5-year survival were all >0.7 (Fig. 5C–E), confirming the model's robustness. Scatter plots also showed a positive correlation between mortality and risk scores, further validating the prognostic model (Fig. 5F,G).

3.6 Tumor Mutational Landscape and Immune Cell Infiltration in Risk-Stratified Populations

Analysis of mutational profiles showed that missense mutations were the main variant type in both risk groups, with higher frequencies of *PIK3CA* and *TP53* mutations in high-risk patients (*TP53*: 48% vs. 11%) (Fig. 6A,B). High-risk tumors had a lower TMB (Fig. 6C,D), suggesting reduced neoantigen production and poorer treatment response. High-risk scores were consistently observed across microsatellite stability (MSS), microsatellite instability low (MSI-L), and MSI-high (MSI-H) subtypes. MSS tumors showed particularly high scores, whereas MSI-H tumors with high mutational load and typically better immunotherapy response were predominantly clustered in the low-risk group (Fig. 6E).

CIBERSORT analysis of immune cell infiltration patterns revealed distinct microenvironment profiles between the two risk groups. Low-risk tumors were characterized by higher proportions of $CD8^+$ T cells, Tregs, and resting DCs, whereas high-risk tumors showed enrichment of naïve B cells, M1 macrophages, activated DCs, and neutrophils (Fig. 6F). TIDE score analysis predicted poorer response to immune checkpoint blockade (ICB) in high-risk patients ($p < 0.05$), indicating greater immune escape potential (Fig. 6G). Analysis with the ESTIMATE algorithm revealed an inverse correlation between risk scores and immune scores (cor <–0.1, $p < 0.05$) (Fig. 6H). The high-risk group showed lower stromal scores and ESTIMATE scores, together with higher tumor purity (Fig. 6I–K), collectively suggesting an immunologically suppressed TME.

3.7 Validation of Prognostic Gene Expression Patterns

Single-cell RNA sequencing of paired tumor and adjacent normal endometrial tissues from one EC patient identified five major cell populations: epithelial cells (epithelial cell adhesion molecule (*EPCAM*), keratin 8 (*KRT8*)), stromal fibroblasts (regulator of G-protein signaling 5 (*RGS5*)), endothelial cells (adhesion G protein-coupled receptor L4 (*ADGRL4*); plasmalemma vesicle associated protein (*PLVAP*)), smooth muscle cells (decorin (*DCN*)), and immune cells (protein tyrosine phosphatase receptor type C (*PTPRC*)) (Fig. 7A,B). UMAP analysis revealed widespread *MTHFD2* expression in non-immune cells, *RPS6KA1* expression in both epithelial and endothelial cells, and scattered *CDKN2A* expression across epithelial, immune, and smooth muscle cells (Fig. 7C). Validation with TCGA-UCEC, GEO, and CPTAC confirmed tumor-upregulated expression of all three genes (Fig. 7D,E). MTHFD2 and CDKN2A were highly expressed in higher-grade tumors and TP53-mutated samples, while RPS6KA1 expression was lower in cases with poor prognosis (Fig. 7F,G). Survival analysis indicated that high *MTHFD2* expression and *CDKN2A* expression were adverse prognostic factors, while downregulation of *RPS6KA1* also predicted poor outcome (Fig. 7H).

3.8 Prognostic Gene-Driven Immunometabolic Classification Reveals Three EC Subtypes

To clarify the roles of prognostic genes in the EC subgroups, we further analyzed their expression and pathway associations. *MTHFD2* and *CDKN2A* were highly expressed in C1, while *RPS6KA1* was highly expressed in C2 (Fig. 8A,B), consistent with the subgroup outcomes. Risk score analysis showed that C1 had the highest scores (Fig. 8C), matching its poor prognosis. GSVA revealed distinct signatures: C1 showed global metabolic suppression (fatty acid, bile acid, cholesterol, hormone signaling) and inhibition of P53, apoptosis, and ROS response, indicating dedifferentiation and immune-metabolic suppression (Fig. 8D). The C1 subgroup also exhibited low $CD8^+$ T/NK infiltration and high CD274/PD-L1 and LAG3, defining an "immune-metabolic suppressed type" with the worst prognosis. C2 featured active proliferation (E2F tran-

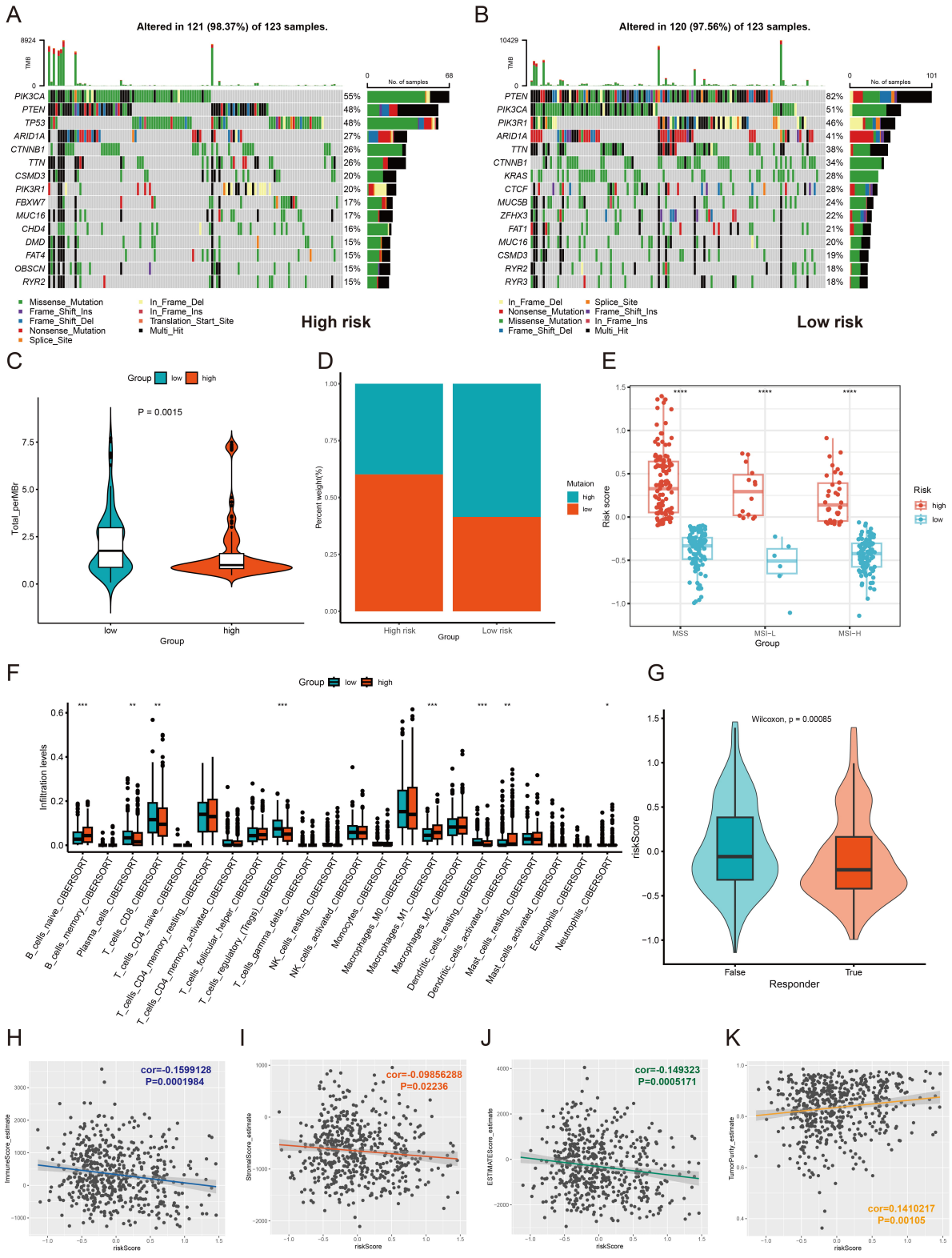

Fig. 6. Analysis of tumor mutations and immune microenvironment infiltration. (A,B) Comparison of mutation frequency and type based on risk scores. (C) Violin plot comparing tumor mutation burden (log2-transformed) between low- and high-risk groups. (D) Bar plot showing the proportion of tumor mutation burden in low- and high-risk groups. (E) Distribution of microsatellite stability subtypes in low- and high-risk groups. (F) Levels of infiltration by different immune cell types. (G) Differential distribution of immune risk scores between responders and non-responders to immunotherapy. (H–K) Correlation analysis between immune-related scores and risk scores. * $p < 0.05$, ** $p < 0.01$, *** $p < 0.001$, **** $p < 0.0001$. MSS, microsatellite stable; MSI-L, microsatellite instability-low; MSI-H, microsatellite instability-high.

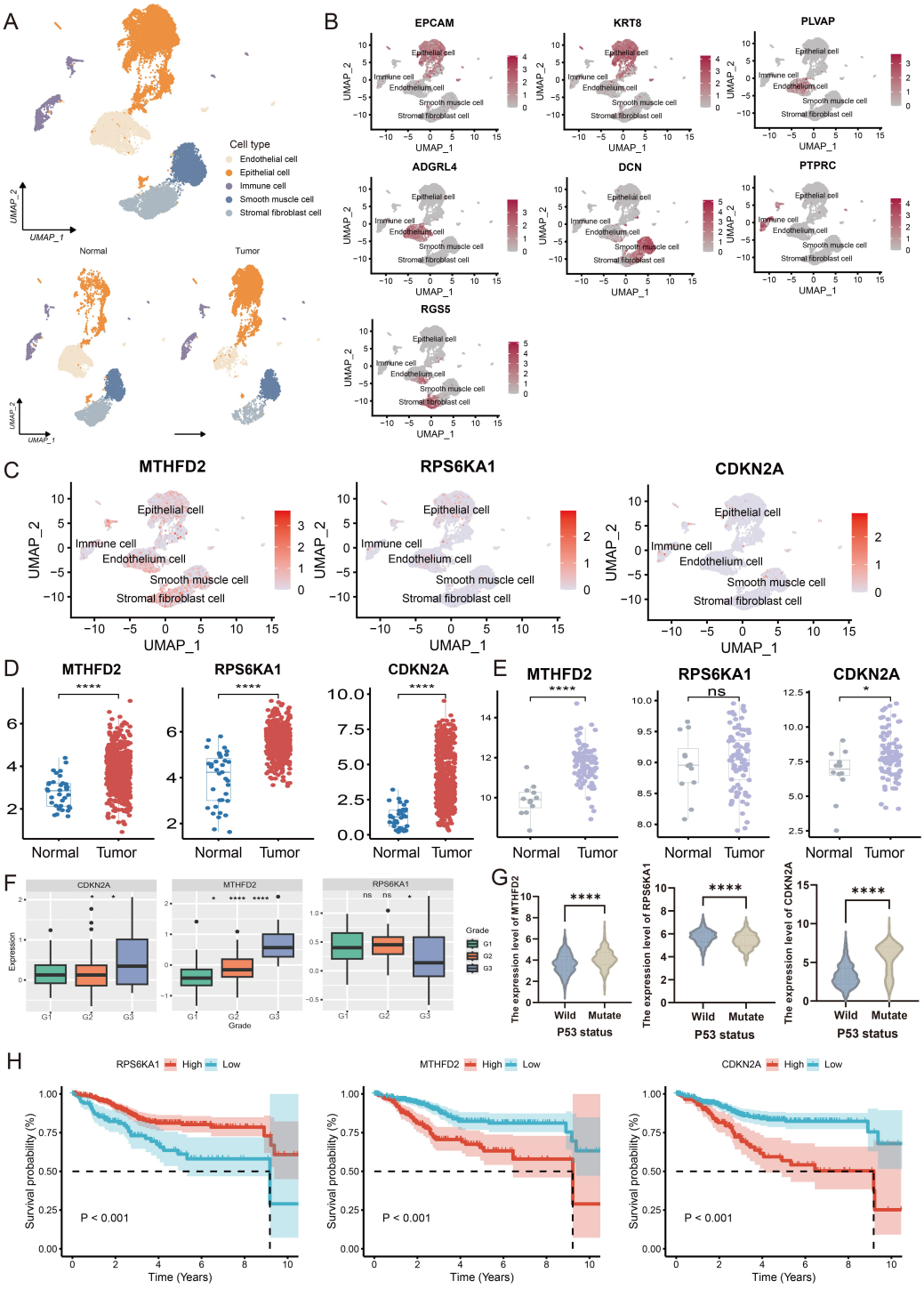

Fig. 7. Validation of prognostic genes in external datasets. (A) UMAP plot displaying five major cell type clusters. (B) UMAP visualization of canonical marker genes across five cell subpopulations. (C) Expression profiles of the three prognostic genes across cell subpopulations. (D,E) Differential expression of the three prognostic genes in TCGA-UCEC and GSE17025 datasets. (F) Expression patterns of the three prognostic genes across different pathological grades in the CPTAC database. (G) Expression levels of the three prognostic genes: comparison between TP53-mutated and wild-type samples. (H) Prediction of disease outcome with the three prognostic genes in the TCGA-UCEC cohort. ns, not significant, * $p < 0.05$, **** $p < 0.0001$. UMAP, uniform manifold approximation and projection; EPCAM, epithelial cell adhesion molecule; KRT8, keratin 8; RGS5, regulator of G-protein signaling 5; ADGRL4, adhesion G protein-coupled receptor L4; PLVAP, plasmalemma vesicle associated protein; DCN, decorin; PTPRC, protein tyrosine phosphatase receptor type C; MTHFD2, methylenetetrahydrofolate dehydrogenase 2; RPS6KA1, ribosomal protein S6 kinase A1; CDKN2A, cyclin-dependent kinase inhibitor 2A.

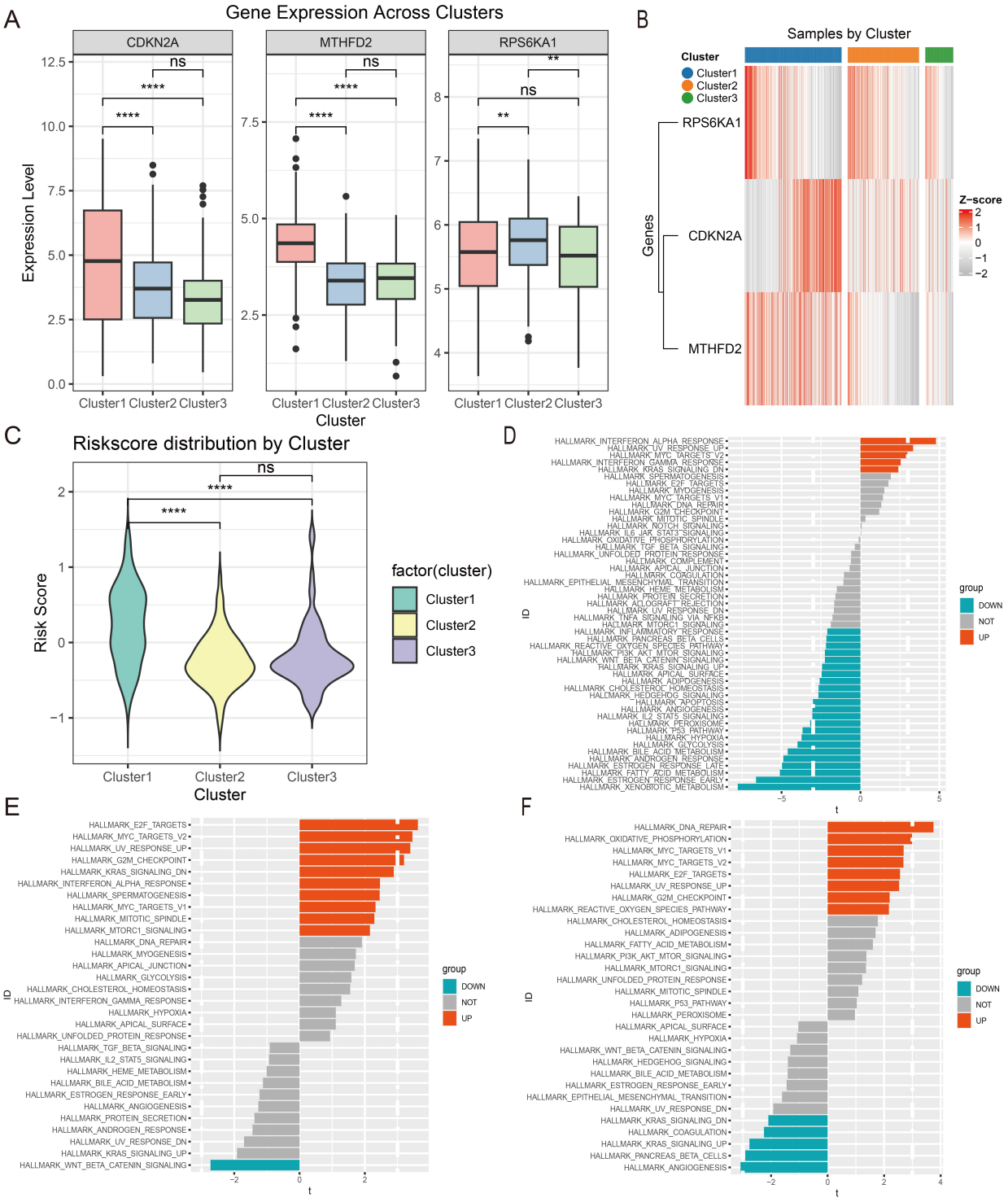

Fig. 8. Redefining the three Gly/Ser/Thr metabolism-related subtypes in EC. (A,B) Expression patterns for the three prognostic genes across the metabolic subtypes are shown as bar plots (A) and heatmaps (B). (C) Distribution of risk scores among the three metabolic subtypes. (D–F) Bar plots showing hallmark pathway enrichment for C1 (D), C2 (E), and C3 (F) subtypes. ns, not significant, ** $p <$ 0.01, **** $p < 0.0001$. C, cluster; *MTHFD2*, methylenetetrahydrofolate dehydrogenase 2; *RPS6KA1*, ribosomal protein S6 kinase A1; *CDKN2A*, cyclin-dependent kinase inhibitor 2A.

scription factor/MYC proto-oncogene, BHLH transcription factor (E2F/MYC) targets, G2/M checkpoint), partial interferon-α/γ activation, and reduced Wnt/β-catenin signaling (Fig. 8E). Despite increased MDSCs, the C2 subgroup had high $CD4^+$ memory T cells, low LAG3/TIGIT, and an immune-balanced state, defining a "proliferation-

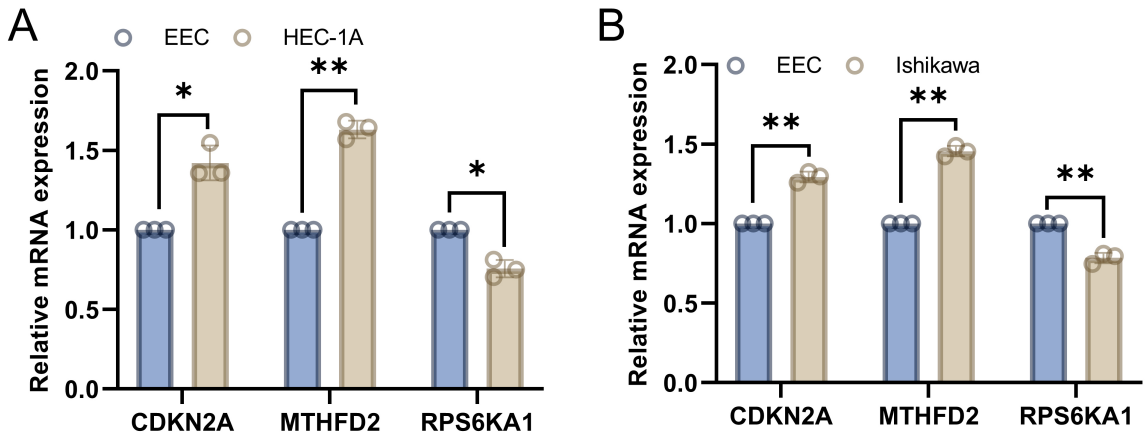

Fig. 9. Validation of the differential expression of key genes *in vitro*. (A) Differential expression of *CDKN2A*, *MTHFD2*, and *RPS6KA1* between EECs and HEC-1A cells. (B) Differential expression of *CDKN2A*, *MTHFD2*, and *RPS6KA1* between EECs and Ishikawa cells. Data are the mean ± SD, with n = 3. Statistical method: paired Student's *t*-test. * $p < 0.05$, ** $p < 0.01$. EECs, endometrial epithelial cells; *MTHFD2*, methylenetetrahydrofolate dehydrogenase 2; *RPS6KA1*, ribosomal protein S6 kinase A1; *CDKN2A*, cyclin-dependent kinase inhibitor 2A.

immune balanced type" with intermediate prognosis. C3 showed upregulated DNA repair and oxidative phosphorylation, but reduced epithelial-mesenchymal transition (EMT), angiogenesis, and KRAS signaling (Fig. 8F). The C3 subtype also had abundant activated $CD8^+$ T and CD56dim NK cells and low IFNGR1/SIGLEC15, indicating an immune-active microenvironment. C3 was therefore defined as a "mitochondrial hypermetabolic-immune activated type" and was linked to better prognosis.

3.9 Differential Expression of Key Genes In Vitro

We next examined differential expression of the key genes (*CDKN2A*, *MTHFD2*, and *RPS6KA*1) *in vitro* by comparing their levels in EECs with those found in EC cell lines (HEC-1A and Ishikawa). Compared with EECs, EC cells showed significantly higher expression of *CDKN2A* and *MTHFD2*, but lower expression of *RPS6KA1* (Fig. 9). These findings provide valuable insights for subsequent investigations.

4. Discussion

Metabolic reprogramming is a key feature of cancer, wherein tumor cells show more active and varied metabolic profiles than normal cells. It is crucial to gain a better understanding of how tumor cells regulate their metabolism, and whether targeting these metabolic needs can result in therapeutic benefit [21]. EC is the second most common malignancy in the female reproductive system and has received increasing attention due to its heterogeneity. Nevertheless, research on the metabolic characteristics of EC remains limited. Our group has shown that upregulation of estrogen-related receptor α, a central energy metabolism regulator, induces cardiolipin-dependent mitochondrial reprogramming in EC cells [22], while also promoting cholesterol metabolism to enhance invasion and metastasis [23]. Although these findings highlight the vital role of energy metabolism in EC, most studies to date have focused on lipid metabolism, with fewer addressing amino acid metabolism.

The present study combined untargeted metabolomics with multi-omics to uncover the role of Gly/Ser/Thr metabolic pathways and their associated genes in EC for the first time. To further evaluate the clinical significance of genes related to Gly/Ser/Thr metabolism, we used Cox and LASSO regression analyses to identify three core prognostic genes (*MTHFD2*, *RPS6KA1*, and *CDKN2A*). These were used to construct a prognostic model for EC.

CDKN2A is a cell cycle regulator. While CDKN2A is usually considered to be a tumor suppressor, emerging evidence suggests that it may also act as an oncogene in some cancer types [24,25]. In thyroid cancer, overexpression of CDKN2A correlates with advanced disease stage and poor prognosis, potentially contributing to immunotherapy resistance and immune evasion [26]. Song *et al.* [27] found elevated CDKN2A expression in lung cancer, along with increased PD-1 and PD-L1 levels, indicating a potential role in tumor immune escape through modulation of immunosuppressive signals. These studies suggest that CDKN2A

could function as an oncogene in certain cancers. Although research on CDKN2A in EC is still limited, Bai *et al*. [28] reported that it may drive tumor initiation and progression by disrupting normal cell cycle regulation. Our study found that CDKN2A is significantly upregulated in EC and associated with poor prognosis. CDKN2A was expressed in epithelial and immune cells, suggesting it has a multifaceted role in EC progression. Mechanistically, aberrant upregulation of CDKN2A in epithelial cells may reflect dysregulated cell cycle control or inactivation of downstream checkpoint pathways, resulting in enhanced tumor cell adaptability. Furthermore, CDKN2A expression in immune cells may be associated with immune dysfunction or immune escape within the TME, potentially facilitating tumor progression through the suppression of effective antitumor immune responses. Therefore, CDKN2A may serve not only as a prognostic biomarker, but also as a potential therapeutic target in EC. Further functional studies are warranted to elucidate the mechanisms by which CDKN2A contributes to tumor progression and immune modulation in EC.

MTHFD2 is involved in one-carbon folate metabolism and metabolic reprogramming. Defective MTHFD2 was found to disrupt mitochondrial glycine synthesis and enhance serine synthesis in breast cancer cells [29]. MTHFD2 overexpression has been reported in several different cancer types [30–32]. It has also been shown to upregulate PD-L1 expression, thus promoting immune evasion by tumors [33]. P53-deficient cells are known to rely on serine for survival [34]. TP53 can suppress MTHFD2, suggesting that upregulation of MTHFD2 could support purine synthesis and redox control in p53-deficient or mutant cells. Targeting of MTHFD2 could therefore have therapeutic potential in patients with p53-mutant tumors [35]. However, there is still only limited research on MTHFD2 in EC. Wu *et al*. [36] reported that MTHFD2 is upregulated in EC, contributing to poor prognosis and promoting EC cell proliferation and invasion. MTHFD2 expression also correlates with immune cell infiltration, and in bladder cancer, it was shown to enrich in cancer immunotherapy by PD1 blockade and associate with immune infiltration [37]. These findings suggest that MTHFD2 plays key roles in tumor progression and immune evasion, making it a potential target for cancer therapy. In the present study, MTHFD2 was widely expressed in EC and emerged as a high-risk factor strongly linked to poor prognosis. We hypothesize that MTHFD2 overexpression in EC contributes to malignant progression and therapy resistance through metabolic reprogramming and immune evasion. Targeting of MTHFD2 could therefore be a promising treatment strategy for p53-mutant EC.

RPS6KA1 is a serine/threonine kinase that generally acts as an oncogene in most cancer types [38–40]. However, Chen *et al*. [41] reported that RPS6KA1 expression is negatively correlated with smoking-related mutational signatures, and that higher RPS6KA1 expression is significantly associated with prolonged overall survival in lung cancer patients. These findings suggest RPS6KA1 may serve as an important prognostic factor and potential therapeutic target in smoking-related lung cancer. Our prognostic analysis identified RPS6KA1 as a protective factor in EC. Low RPS6KA1 expression predicted worse outcomes in external validation datasets. However, RPS6KA1 was upregulated in bulk tumor transcriptomic data, but downregulated in EC cell lines compared with EECs. This discrepancy may be due to the capture of the TME in tissue-based analyses, but its absence in the cell line models used *in vitro*. Further validation in clinical tissue samples will be performed in future studies.

Our study introduces a multi-gene prognostic model based on Gly/Thr/Ser metabolism-related genes (*MTHFD2*, *RPS6KA1*, and *CDKN2A*) to stratify patients into distinct risk groups. High-risk patients showed significantly worse prognosis, with the model demonstrating excellent predictive accuracy. This was validated by TCGA data and our proteomic datasets, and supported by ROC curves, K-M survival analyses, and risk score distributions. The integration of risk scores with molecular subtypes highlighted the strong stratification ability of our model, and emphasized the key roles of MTHFD2, RPS6KA1, and CDKN2A in determining EC prognosis. Further analyses of the TMB, immune microenvironment, and immune scores revealed that high-risk patients had more frequent TP53 mutations, higher TIDE scores, lower immune and stromal scores, and higher tumor purity. These findings indicate the presence of an immunologically “cold” TME in high-risk patients, which is associated with poorer immunotherapy responses.

We also performed cluster analysis based on gene modules from WGCNA, integrating prognostic gene expression with immune features. Using GSVA and survival analysis, we identified three EC subgroups with distinct molecular and clinical prognostic differences: immune-metabolic suppressed (C1), proliferation-immune balanced (C2), and immune-activated (C3). The C1 subgroup had the worst prognosis and showed metabolic pathway suppression and an “immune-cold” environment (low $CD8^+$ T cell and DC infiltration, high PD-L1 and LAG3 expression). A key driver of EC progression is MTHFD2-mediated one-carbon metabolism abnormality, which induces mitochondrial DNA damage, provides the tumor with its energy needs, impairs immune function, and promotes immune escape [42,43]. High MTHFD2 expression in C1 supports this mechanism, suggesting that targeting this enzyme could reverse immune suppression in C1 subtype EC. The C2 subtype offers a novel perspective on EC heterogeneity, with these tumors showing high proliferation and active anti-tumor immunity. This balance state may be key to their favorable prognosis, since increased proliferative signals are effectively counterbalanced by the immune system, thus preventing excessive tumor growth while maintaining microenvironmental homeostasis [44]. And Defects in DNA repair can result in the loss of genomic stability,

contributing to tumorigenesis and mutation accumulation [45]. A previous study showed that metabolic syndrome and estrogen in type I EC cells can drive metabolic reprogramming by inhibiting OXPHOS, thereby promoting EC proliferation [46]. The C3 EC subgroup in the present study showed upregulated DNA repair signaling and OXPHOS pathways, along with activated $CD8^+$ T cells and DCs, indicating a favorable prognosis. In summary, the EC subgroup classification system developed in the current study highlights the importance of metabolism and immune interactions in EC progression, as well as providing guidance for clinical precision medicine. C1 EC patients may need combined metabolic intervention (e.g., MTHFD2 inhibition) and immunotherapy (e.g., anti-PD-L1) to reverse immune suppression. C2 EC patients may benefit from ICBs to enhance their immune-balanced state, while C3 patients may require maintenance therapy to preserve their metabolic maturity and immune-activated advantages. Future mechanistic studies and clinical trials targeting key molecules in each subtype may provide further validation of this system and lead to more precise treatment options for EC patients. Our novel classification system not only clarifies the metabolic-immune interactions driving EC progression, but also provides insights for personalized treatment strategies. However, several limitations of this study should be acknowledged. First, the transcriptomic and clinical data used for model construction and validation were primarily derived from retrospective public datasets. This may introduce selection bias and limit causal inference, underscoring the need for future prospective validation. Second, although our study integrated metabolomics, transcriptomics, proteomics, and single-cell analyses to identify prognostic genes, functional mechanistic assays were not performed. Further *in vitro* and *in vivo* experiments are therefore required to elucidate the biological roles of MTHFD2, RPS6KA1, and CDKN2A in EC progression and immune regulation. Finally, the untargeted metabolomics analysis was conducted with a relatively small sample size, which may restrict statistical power and generalizability. Larger independent cohorts will be needed for further validation.

5. Conclusions

This study is the first to demonstrate a strong link between EC development and the Gly/Ser/Thr metabolic pathways. By analyzing genes within this pathway, we developed a prognostic model based on the expression of *MTHFD2*, *RPS6KA1*, and *CDKN2A*. This model showed high predictive accuracy and clinical relevance. Additionally, we established a molecular classification system that integrates metabolic and immune features, thus identifying novel biomarkers and potential therapeutic targets for the precision treatment of EC.

Abbreviations

EC, Endometrial cancer; Gly/Ser/Thr, Glycine/Serine/Threonine; WGCNA, Weighted Gene Co-Expression Network Analysis; MTHFD2, Methylenetetrahydrofolate dehydrogenase/cyclohydrolase 2; RPS6KA1, Ribosomal protein S6 kinase A1; CDKN2A, Cyclin-dependent kinase inhibitor 2A; GSVA, Gene set variation analysis; KEGG, Kyoto Encyclopedia of Genes and Genomes; GEO, Gene Expression Omnibus; UCEC, Uterine Corpus Endometrial Carcinoma; LASSO, Least absolute shrinkage and selection operator; ROC, Receiver operating characteristic; TMB, Tumor mutation burden; TIDE, Tumor immune dysfunction and exclusion; UMAP, Uniform manifold approximation and projection; MDSCs, Myeloid-derived suppressor cells.

Availability of Data and Materials

The datasets used and analyzed during the current study are available from the corresponding author on reasonable request.

Author Contributions

JXY conducted the experiments, analyzed the data, and wrote the manuscript. YSS collected and analyzed the data and provided valuable discussions. MTZ and XTL performed the data management. XDM and PMS conceived the study, contributed to the critical revision of the article for important intellectual content, supervised the research, and provided financial support. All authors gave final approval for the submitted version and agreed to take responsibility for all aspects of the work. All authors contributed to editorial changes in the manuscript.

Ethics Approval and Consent to Participate

All subjects gave written informed consent to participate in the study. The study was conducted in accordance with the Declaration of Helsinki and approved by Fujian Maternity and Child Health Hospital Ethics Commission (Grant NO. 2021KRD001).

Acknowledgment

We gratefully acknowledge Director Yan Lin and Prof. Hao Lin for generously providing patient clinical specimens and associated clinical data, as well as for their financial support.

Funding

This research was funded by the Fujian Province Central Government-Guided Local Science and Technology Development Project (No. 2023L3019), the Fujian Province health medicine innovation project (No. 2024CXB008), Joint Fundsfor the Innovation of Science and Technology (No. 2024Y9585), Fujian Provincial Nature Science Foundation of China (No. 2023J011232) and

Fujian Province and the Startup Fund for scientific research, Fujian Medical University (No. 2023QH2045).

Conflict of Interest

The authors declare no conflict of interest.

Supplementary Material

Supplementary material associated with this article can be found, in the online version, at https://doi.org/10.31083/FBL48779.

References

[1] Siegel RL, Miller KD, Wagle NS, Jemal A. Cancer statistics, 2023. CA: A Cancer Journal for Clinicians. 2023; 73: 17–48. https://doi.org/10.3322/caac.21763.

[2] Siegel RL, Giaquinto AN, Jemal A. Cancer statistics, 2024. CA: a Cancer Journal for Clinicians. 2024; 74: 12–49. https://doi.org/10.3322/caac.21820.

[3] Gordhandas S, Zammarrelli WA, Rios-Doria EV, Green AK, Makker V. Current Evidence-Based Systemic Therapy for Advanced and Recurrent Endometrial Cancer. Journal of the National Comprehensive Cancer Network: JNCCN. 2023; 21: 217–226. https://doi.org/10.6004/jnccn.2022.7254.

[4] Li Z, Zhang H. Reprogramming of glucose, fatty acid and amino acid metabolism for cancer progression. Cellular and Molecular Life Sciences: CMLS. 2016; 73: 377–392. https://doi.org/10.1007/s00018-015-2070-4.

[5] Kanai Y. Amino acid transporter LAT1 (SLC7A5) as a molecular target for cancer diagnosis and therapeutics. Pharmacology & Therapeutics. 2022; 230: 107964. https://doi.org/10.1016/j.pharmthera.2021.107964.

[6] Jiang H, Zhang N, Tang T, Feng F, Sun H, Qu W. Target the human Alanine/Serine/Cysteine Transporter 2(ASCT2): Achievement and Future for Novel Cancer Therapy. Pharmacological Research. 2020; 158: 104844. https://doi.org/10.1016/j.phrs.2020.104844.

[7] Chen Y, Feng X, Wu Z, Yang Y, Rao X, Meng R, *et al*. USP9X-mediated REV1 deubiquitination promotes lung cancer radioresistance via the action of REV1 as a Rad18 molecular scaffold for cystathionine γ-lyase. Journal of Biomedical Science. 2024; 31: 55. https://doi.org/10.1186/s12929-024-01044-3.

[8] Huang K, Xie W, Wang S, Li Q, Wei X, Chen B, *et al*. High SPINK1 Expression Predicts Poor Prognosis and Promotes Cell Proliferation and Metastasis of Hepatocellular Carcinoma. Journal of Investigative Surgery: the Official Journal of the Academy of Surgical Research. 2021; 34: 1011–1020. https://doi.org/10.1080/08941939.2020.1728443.

[9] Kanehisa M, Furumichi M, Sato Y, Matsuura Y, Ishiguro-Watanabe M. KEGG: biological systems database as a model of the real world. Nucleic Acids Research. 2025; 53: D672–D677. https://doi.org/10.1093/nar/gkae909.

[10] Kanehisa M. Toward understanding the origin and evolution of cellular organisms. Protein Science: a Publication of the Protein Society. 2019; 28: 1947–1951. https://doi.org/10.1002/pro.3715.

[11] Kanehisa M, Goto S. KEGG: kyoto encyclopedia of genes and genomes. Nucleic Acids Research. 2000; 28: 27–30. https://doi.org/10.1093/nar/28.1.27.

[12] Langfelder P, Horvath S. WGCNA: an R package for weighted correlation network analysis. BMC Bioinformatics. 2008; 9: 559. https://doi.org/10.1186/1471-2105-9-559.

[13] Ritchie ME, Phipson B, Wu DI, Hu Y, Law CW, Shi W, *et al*. limma powers differential expression analyses for RNA-sequencing and microarray studies. Nucleic Acids Research. 2015; 43: e47.

[14] Wilkerson MD, Hayes DN. ConsensusClusterPlus: a class discovery tool with confidence assessments and item tracking. Bioinformatics (Oxford, England). 2010; 26: 1572–1573. https://doi.org/10.1093/bioinformatics/btq170.

[15] Blanche P, Dartigues JF, Jacqmin-Gadda H. Estimating and comparing time-dependent areas under receiver operating characteristic curves for censored event times with competing risks. Statistics in Medicine. 2013; 32: 5381–5397. https://doi.org/10.1002/sim.5958.

[16] Newman AM, Liu CL, Green MR, Gentles AJ, Feng W, Xu Y, *et al*. Robust enumeration of cell subsets from tissue expression profiles. Nature Methods. 2015; 12: 453–457. https://doi.org/10.1038/nmeth.3337.

[17] Liu Y, Zhao Y, Song H, Li Y, Liu Z, Ye Z, *et al*. Metabolic reprogramming in tumor immune microenvironment: Impact on immune cell function and therapeutic implications. Cancer Letters. 2024; 597: 217076. https://doi.org/10.1016/j.canlet.2024.217076.

[18] Xia L, Oyang L, Lin J, Tan S, Han Y, Wu N, *et al*. The cancer metabolic reprogramming and immune response. Molecular Cancer. 2021; 20: 28. https://doi.org/10.1186/s12943-021-01316-8.

[19] Szanto A, Balint BL, Nagy ZS, Barta E, Dezso B, Pap A, *et al*. STAT6 transcription factor is a facilitator of the nuclear receptor PPARγ-regulated gene expression in macrophages and dendritic cells. Immunity. 2010; 33: 699–712. https://doi.org/10.1016/j.immuni.2010.11.009.

[20] Zhou J, Tison K, Zhou H, Bai L, Acharyya RK, McEachern D, *et al*. STAT5 and STAT3 balance shapes dendritic cell function and tumour immunity. Nature. 2025; 643: 519–528. https://doi.org/10.1038/s41586-025-09000-3.

[21] Finley LWS. What is cancer metabolism? Cell. 2023; 186: 1670–1688. https://doi.org/10.1016/j.cell.2023.01.038.

[22] Ma J, Mao X, Ren Y, Lin X, Wu Q, Zhang M, *et al*. Antagonism of estrogen-related receptor-α inhibits mitochondrial oxidative phosphorylation and reduces M2 macrophage infiltration in endometrial cancer. Journal for Immunotherapy of Cancer. 2025; 13: e012521. https://doi.org/10.1136/jitc-2025-012521.

[23] Tang S, Ma J, Su P, Lei H, Tong Y, Cai L, *et al*. ERRα Up-Regulates Invadopodia Formation by Targeting HMGCS1 to Promote Endometrial Cancer Invasion and Metastasis. International Journal of Molecular Sciences. 2023; 24: 4010. https://doi.org/10.3390/ijms24044010.

[24] Dong Y, Zheng M, Wang X, Yu C, Qin T, Shen X. High expression of CDKN2A is associated with poor prognosis in colorectal cancer and may guide PD-1-mediated immunotherapy. BMC Cancer. 2023; 23: 1097. https://doi.org/10.1186/s12885-023-11603-w.

[25] Gu R, Li S, Yu B, Gu J, Guan B, Wu H. Increased CDKN2A expression correlates with resistance to platinum-based therapy and decreased infiltration of B lymphocytes in colon adenocarcinoma. Functional & Integrative Genomics. 2025; 25: 144. https://doi.org/10.1007/s10142-025-01657-3.

[26] Xie K, Hong X, Ren X, Tong Z. Multi-omics characterization of prognostic signature and novel molecular subtypes associated with anoikis and in vitro validation of CDKN2A in thyroid carcinoma. Phytomedicine: International Journal of Phytotherapy and Phytopharmacology. 2025; 145: 156956. https://doi.org/10.1016/j.phymed.2025.156956.

[27] Song T, Li S, Zhao K, Zou D, Zhang M, Wang H. Comprehensive analysis of prognosis and tumor immune microenvironment of cuproptosis-related gene CDKN2A in lung adenocarcinoma. BMC Pulmonary Medicine. 2025; 25: 179. https://doi.org/10.1186/s12890-025-03631-y.

[28] Bai Y, Luo S, Shuai R, Zhang X, Yuan L, Liu D. Exploration of shared pathogenic factors and causative genes in early-stage endometrial cancer and osteoarthritis. Scientific Reports. 2025; 15: 22123. https://doi.org/10.1038/s41598-025-04470-x.

[29] Koufaris C, Gallage S, Yang T, Lau CH, Valbuena GN, Keun HC. Suppression of MTHFD2 in MCF-7 Breast Cancer Cells Increases Glycolysis, Dependency on Exogenous Glycine, and Sensitivity to Folate Depletion. Journal of Proteome Research. 2016; 15: 2618–2625. https://doi.org/10.1021/acs.jproteome.6b00188.

[30] Cui X, Su H, Yang J, Wu X, Huo K, Jing X, *et al*. Up-regulation of MTHFD2 is associated with clinicopathological characteristics and poor survival in ovarian cancer, possibly by regulating MOB1A signaling. Journal of Ovarian Research. 2022; 15: 23. https://doi.org/10.1186/s13048-022-00954-w.

[31] Mo J, Gao Z, Zheng L, Yan M, Xue M, Xu J, *et al*. Targeting mitochondrial one-carbon enzyme MTHFD2 together with pemetrexed confers therapeutic advantages in lung adenocarcinoma. Cell Death Discovery. 2022; 8: 307. https://doi.org/10.1038/s41420-022-01098-y.

[32] Wang J, Yu Z, Jiang Y, Le T, Wu Y, Li Z, *et al*. Downregulation of MTHFD2 Inhibits Proliferation and Enhances Chemosensitivity in Hepatocellular Carcinoma via PI3K/AKT Pathway. Frontiers in Bioscience (Landmark Edition). 2024; 29: 35. https://doi.org/10.31083/j.fbl2901035.

[33] Shang M, Yang H, Yang R, Chen T, Fu Y, Li Y, *et al*. The folate cycle enzyme MTHFD2 induces cancer immune evasion through PD-L1 up-regulation. Nature Communications. 2021; 12: 1940. https://doi.org/10.1038/s41467-021-22173-5.

[34] Maddocks ODK, Berkers CR, Mason SM, Zheng L, Blyth K, Gottlieb E, *et al*. Serine starvation induces stress and p53-dependent metabolic remodelling in cancer cells. Nature. 2013; 493: 542–546. https://doi.org/10.1038/nature11743.

[35] Li G, Wu J, Li L, Jiang P. p53 deficiency induces MTHFD2 transcription to promote cell proliferation and restrain DNA damage. Proceedings of the National Academy of Sciences of the United States of America. 2021; 118: e2019822118. https://doi.org/10.1073/pnas.2019822118.

[36] Wu S, Cai W, Li Y, Tan W, Yuan Y, Zhou Z, *et al.* SNHG3/hsa-miR-455-5p axis-mediated high expression of MTHFD2 correlates with tumor immune infiltration and endometrial carcinoma progression. International Journal of Medical Sciences. 2023; 20: 1097–113. https://doi.org/10.7150/ijms.81962.

[37] Zhu L, Liu X, Zhang W, Hu H, Wang Q, Xu K. MTHFD2 is a potential oncogene for its strong association with poor prognosis and high level of immune infiltrates in urothelial carcinomas of bladder. BMC Cancer. 2022; 22: 556. https://doi.org/10.1186/s12885-022-09606-0.

[38] Yu G, Lee YC, Cheng CJ, Wu CF, Song JH, Gallick GE, *et al*. RSK promotes prostate cancer progression in bone through ING3, CKAP2, and PTK6-mediated cell survival. Molecular Cancer Research: MCR. 2015; 13: 348–357. https://doi.org/10.1158/1541-7786.MCR-14-0384-T.

[39] Casalvieri KA, Matheson CJ, Backos DS, Reigan P. Selective Targeting of RSK Isoforms in Cancer. Trends in Cancer. 2017; 3: 302–312. https://doi.org/10.1016/j.trecan.2017.03.004.

[40] Kong T, Laranjeira ABA, Letson CT, Yu L, He F, Jayanthan A, *et al*. RSK1 dependency in FLT3-ITD acute myeloid leukemia. Blood Cancer Journal. 2024; 14: 207. https://doi.org/10.1038/s41408-024-01187-4.

[41] Chen Z, Wen W, Cai Q, Long J, Wang Y, Lin W, *et al*. From tobacco smoking to cancer mutational signature: a mediation analysis strategy to explore the role of epigenetic changes. BMC Cancer. 2020; 20: 880. https://doi.org/10.1186/s12885-020-07368-1.

[42] Martínez-Jiménez F, Chowell D. Genetic immune escape in cancer: timing and implications for treatment. Trends in Cancer. 2025; 11: 286–294. https://doi.org/10.1016/j.trecan.2024.11.002.

[43] Demicco M, Liu XZ, Leithner K, Fendt SM. Metabolic heterogeneity in cancer. Nature Metabolism. 2024; 6: 18–38. https://doi.org/10.1038/s42255-023-00963-z.

[44] Spitschak A, Dhar P, Singh KP, Casalegno Garduño R, Gupta SK, Vera J, *et al*. E2F1-induced autocrine IL-6 inflammatory loop mediates cancer-immune crosstalk that predicts T cell phenotype switching and therapeutic responsiveness. Frontiers in Immunology. 2024; 15: 1470368. https://doi.org/10.3389/fimmu.2024.1470368.

[45] Hopkins JL, Lan L, Zou L. DNA repair defects in cancer and therapeutic opportunities. Genes & Development. 2022; 36: 278–293. https://doi.org/10.1101/gad.349431.122.

[46] Li J, Yang H, Zhang L, Zhang S, Dai Y. Metabolic reprogramming and interventions in endometrial carcinoma. Biomedicine & Pharmacotherapy = Biomedecine & Pharmacotherapie. 2023; 161: 114526. https://doi.org/10.1016/j.biopha.2023.114526.